

A Simple Surfactant-Free Solution Phase Synthesis of Flower-like In_2S_3 Hierarchitectures and their Photocatalytic Activities

Rengaraj Selvaraj^{1*}, Kezhen Qi², Uiseok Jeong³, Kholood Al Nofli¹, Salma Al-Kindy¹, Mika Sillanpää⁴, and Younghun Kim³.

¹Department of Chemistry, College of Science, Sultan Qaboos University, Muscat, Al- Khodh 123, Sultanate of Oman. ²College of Chemistry and Life Science, Shenyang Normal University, Shenyang, 110034, China. ³Department of Chemical Engineering, Kwangwoon University, Seoul 139-701, Korea. ⁴Laboratory of Green Chemistry, LUT Savo Sustainable Technologies, Lappeenranta University of Technology, Sammonkatu 12, FI-50130 Mikkeli, Finland. *Email: rengaraj@squ.edu.om.

ABSTRACT: Flower-like In_2S_3 hierarchical nanostructures were successfully prepared *via* a facile solution-phase route, using thiacetamide as both sulfur source and capping agent. Our experimental results demonstrated that the morphology of these In_2S_3 nanostructures can be easily modified by changing the ratio of $\text{In}(\text{NO}_3)_3$ /thiacetamide. With the ratio increasing from 1:1.5 to 1:6, the In_2S_3 crystals exhibited flower-like morphology of varying size. XRD and HRTEM of the flowers revealed the cubic structure of In_2S_3 ; morphological studies examined by SEM and TEM showed that the synthesized In_2S_3 nanostructure was a flower-like hierarchitectures assembled from nanoscale flakes. XPS and EDX analysis confirmed the stoichiometry of In_2S_3 nanoflowers. The optical properties were investigated by UV-vis DRS, which indicated that the In_2S_3 nanoflower samples possess a band gap from 1.90 to 1.97 eV. Furthermore, photocatalytic activity studies revealed that the prepared In_2S_3 nanoflowers exhibit an excellent photocatalytic performance, degrading rapidly the aqueous methylene blue dye solution under visible light irradiation. These results suggest that In_2S_3 nanoflowers will be a promising candidate for a photocatalyst working under the visible light range.

Keywords: In_2S_3 nanoflowers; Solution-phase synthesis; Capping agent; Photocatalyst.

طريقة بسيطة لتركيب كبريت الأنديموم (In_2S_3) الوردي الشكل والمتعالي الهندسة عبر محلول خال من السطوح الفاعلة وظائف المركب التحفيزية الضوئية.

رنجراج سلفراج ، كيزن كي، ويسوك جيونغ، خلود النوفلية، سلمى الكندية، ميكاسيلانبا و يونغون كيم

ملخص: تم بنجاح تركيب كبريت الأنديموم In_2S_3 الوردي الشكل والمتعالي التركيب النانوي من خلال طبقة المحلول وذلك باستعمال thioacetamide كمصدر للكبريت وعامل موقف للتفاعل. وقد أثبتت نتائجنا الاختبارية أن الشكل العام لهذه المركبات النانوية يمكن تعديله بسهولة من خلال تغيير نسبة $\text{In}(\text{NO}_3)_3$ /thioacetamide مع زيادة النسبة من 1: 1.5 إلى 1:6، اتخذت بلورات In_2S_3 شكلها الوردي بأحجام مختلفة. وخلال أشعة "X" والمجهر الإلكتروني أثبتت النتائج أن In_2S_3 النانوي الحجم مركب بشكل وردي متعالي التركيب ومؤلف من شرائح نانوية. وقد أثبتت التحاليل أيضاً العلاقات الوزنية في In_2S_3 . وقد أشارت أبحاثنا الضوئية المرئية والما فوق البنفسجية أن الخصائص البصرية ل In_2S_3 الوردي النانوي تتمتع بشفرة شريطية من 1.90 إلى 1.97 electron volt. إضافة إلى إن الخصائص التحفيزية الضوئية ل In_2S_3 أثبتت بأنها ممتازة الأداء بعد أن تم بسرعة تقويض وتكسير مادة ال methylene الأزرق المذاب في الماء تحت أشعة ضوئية مرئية. هذه النتائج تقترح بأن ال In_2S_3 الوردي النانوي هو مرشح واعد للتحفيز الضوئي تحت أشعة مرئية.

مفتاح الكلمات: In_2S_3 نانو وردي الشكل، تركيب محلولي، العامل الموقف التحفيز الضوئي.

1. Introduction

The rational design and fabrication of nanomaterials with special morphologies of nanostructures have attracted a great deal of attention because the properties of a material depend not only on its phase, shape and size, but also on its organization [1,2]. In particular, controlled hierarchical semiconductor nanostructures have attracted much attention because of their potential in new applications in catalysis [3], solar cells [4], chemical sensors [5], and supercapacitors [6]. Thus, controllable synthesis of hierarchical nanostructures is of great interest and urgently called

for. At present, scientists have been devoting considerable efforts to three dimensional (3D) hierarchical architectures assembled by the low dimensional nanoscale building blocks, such as nanoplates, nanoparticles, nanorods, and so forth [7,8]. However, it is still important, from the perspective of both science and industry, to develop a simple method to fabricate 3D hierarchical nanostructures with desired structures and properties and to explore their potential applications.

Indium sulfide (In_2S_3), as an important semiconductor material, has stimulated great interest because of its wide applications in optical [9], photoconductive [10], optoelectronic [11] and catalytic fields [12]. These applications result from its unique physicochemical properties, which depend not only on its phase but also on its shape and organization. For instance, Liu *et al.* [13] have reported that $\beta\text{-In}_2\text{S}_3$ nanotubes showed high photocatalytic performance on the decomposition of Rhodamine B under solar irradiation. Du *et al.* [14] have synthesized ultrathin $\beta\text{-In}_2\text{S}_3$ nanobelts *via* an improved hydrothermal route, and found that these showed a good photocatalytic performance on the degradation of methylene blue (MB). Moreover, $\beta\text{-In}_2\text{S}_3$ hollow microspheres also exhibited an excellent photocatalytic performance in degrading MB under visible light irradiation [15]. These results suggest that In_2S_3 with various morphologies is a promising candidate for photocatalysis under visible light. So far, considerable effort has been devoted to fabricating various morphologies, including particles [16], flakes [17], wires [18], tubes [19], belts [20], spheres [21], sheets [22], dendrites [23] and so on. Despite these advances having been made, the ability to synthesize 3D In_2S_3 hierarchical architectures with fine morphology control still remains a significant challenge.

In this paper, we present a facile solution-phase synthesis of 3D flower-like $\beta\text{-In}_2\text{S}_3$ hierarchical nanostructures, which are composed of two-dimensional (2D) nanosheets. Flower-like In_2S_3 architectures can be obtained only using thioacetamide as both a sulfur source and a capping agent. The effect of molar ratios of precursors on the morphologies of flower-like In_2S_3 architectures and their formation mechanism are also discussed. Furthermore, optical and photocatalytic properties of the flower-like nanostructures are also reported.

2. Experimental section

2.1 Material preparation

The flower-like In_2S_3 nanocrystals were synthesized using analytical grade indium nitrate $\text{In}(\text{NO}_3)_3 \cdot 5\text{H}_2\text{O}$ (Sigma-Aldrich 99%) and thioacetamide (TAA) ($\text{C}_2\text{H}_5\text{NS}$) (Sigma-Aldrich 99%). As a typical synthesis, 10 mmol of $\text{In}(\text{NO}_3)_3 \cdot 5\text{H}_2\text{O}$ and 15-60 mmol (1:1.5 to 1:6 molar ratio of $\text{In}(\text{NO}_3)_3$ to $\text{C}_2\text{H}_5\text{NS}$) of TAA were dissolved in 100 mL of deionized water and continuously stirred for 30 min to form a homogenous solution. The above mixture was then transferred to a round bottomed flask and refluxed at 105 °C for 30 min, which yielded an orange precipitate. The product was collected by centrifugation, washed with deionized water and ethanol several times, and dried at 70 °C for 24 h. The final product was calcined at 350 °C for 2h for further characterization.

2.2 Material characterization

The products were characterized by X-ray diffraction (XRD) using a Bruker (D5005) X-ray diffractometer equipped with graphite monochromatized CuK_α radiation ($\lambda = 1.54056 \text{ \AA}$). Morphology observations were performed on a Hitachi S-4800 field-emission scanning electron microscope. The morphologies and microstructures of the prepared products were analyzed by the transmission electron microscope (TEM) (JEOL JEM-3010). The chemical states of the samples were studied by X-ray photoelectron spectroscopy (XPS). The X-ray source was AlK_α radiation (1.4867 eV). The photo-emitted electrons which escaped from the sample were analyzed in a hemispherical energy analyzer at a pass energy of $E_p = 20 \text{ eV}$. All spectra were obtained with an energy step of 0.1 eV and a dwell time of 50 ms. The absorption spectrum of the samples in the diffused reflectance spectrum (DRS) mode was recorded in the wavelength range of 200 and 1000 nm using a spectrophotometer (Jasco-V670), with BaSO_4 as a reference.

All photoreaction experiments were carried out in a photocatalytic reactor system, which consisted of a cylindrical borosilicate glass reactor vessel with an effective volume of 500 mL, a cooling water jacket, and a 150 W sodium vapor lamp (OSRAM Vialox NAV-TS Super 150 W) positioned axially at the center as a visible light source. The reaction temperature was kept at 20 °C by cooling water. A special glass frit was fixed at the reactor as an air diffuser to disperse air uniformly into the solution.

Photocatalytic activities of the prepared samples were examined by the degradation of methylene blue under visible light irradiation. For each run the reaction suspension was freshly prepared by adding 0.10 g of catalyst into 250 mL of aqueous methylene blue solution, with an initial concentration of 5 mg L^{-1} . Prior to the photoreaction, the suspension was magnetically stirred under dark conditions for 30 min to attain the adsorption/desorption equilibrium condition. The aqueous suspension containing methylene blue and photocatalyst was then irradiated under visible light with constant aeration. At the 10-min intervals, the analytical sample was taken from the suspension, immediately centrifuged at 4000 revolutions per minute (rpm) for 15 min, and then filtered to remove the catalyst. The filtrate was analyzed by using an ultraviolet-visible (UV-vis) spectrophotometer (Perkin-Elmer Lambda 45), and the concentration of MB was monitored at 664 nm.

3. Results and discussion

3.1 The morphology and crystal structure of the products

Figure 1a shows the XRD pattern of the prepared product from the $\text{In}(\text{NO}_3)_3/\text{C}_2\text{H}_5\text{NS}$ molar ratio of 1:6. The peaks were indexed to a cubic phase of $\beta\text{-In}_2\text{S}_3$ (JCPDS card No. 65-0459). The morphologies and structures of the product were examined with TEM and high-resolution TEM (HRTEM). Figure 1b shows the flower-like $\beta\text{-In}_2\text{S}_3$ hierarchitectures in a large area, while an individual flower-like hierarchitectures shown in Figure 1c is about 300-350 nm in diameter. It can be seen that the hierarchitectures are constructed from the aggregation of many thin petal-like building units. The nanopetals are of layered structure and consist of the nanoflakes growing on both sides uniformly. The HRTEM image (Figure 1d) of individual nanopetals indicates a high degree of crystallinity of In_2S_3 nanoflowers. The distance between adjacent lattice planes is about 0.27 nm, corresponding to the (400) plane. Furthermore, the EDX spectrum recorded from the highlighted region in Figure 1c confirms that the components of the products are only In and S with a ratio of 2.02:3 (Figure 3g), which is consistent with the XRD result above. The Cu signal is attributed to the TEM copper supporting grid. The elemental mapping of In and S did not show a strong composition variation (Figures 1e and 1f). The contrast difference was contributed by the morphology of the selected petals only.

To confirm the composition of the In_2S_3 nanoflowers, XPS analysis was carried out (Figure 2). The binding energies obtained in the XPS analysis were corrected for specimen charging by referencing the C 1s to 284.6 eV. The survey XPS spectrum is shown in Figure 2a. No peak of any element other than C, O, In, and S was observed. The observed C peak is due to the carbon supporting film on the copper TEM grid, and the O peaks can be attributed to the absorption of oxygen on the sample surface and the carbon supporting film. The XPS spectra of the In_2S_3 sample is consistent with the typical In_2S_3 spectrum reported in the literature [24]. Figures 2b and 2c show the high-resolution XPS spectra of In 3d and S 2p, respectively. The two strong peaks at 445.3 and 452.6 eV are assigned to the binding energies of In $3d_{5/2}$ and In $3d_{3/2}$. The observed peaks at 160.9 and 162.4 eV are attributed to the binding energy of S $2p_{3/2}$ and S 2p. These values are in good agreement with the reported data [25]. According to the measurements of the In 3d and S 2p peak areas, the atomic ratio of In/S is 2:3, very close to the nominal composition of In_2S_3 , which further confirms that the final products were stoichiometric In_2S_3 with no impurity. This result is consistent with the measurements of energy-dispersive X-ray (EDX) and with the element map. (see Figures 1e-g).

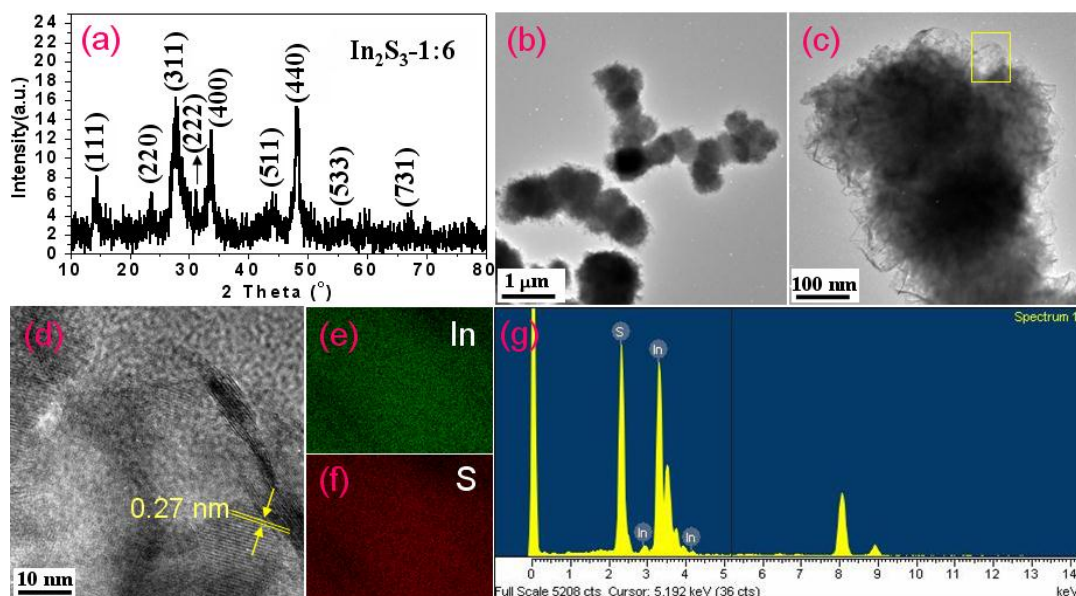


Figure 1. Characterizations of prepared In_2S_3 nanoflowers from the $\text{In}(\text{NO}_3)_3/\text{C}_2\text{H}_5\text{NS}$ molar ratio of 1:6. (a) XRD patterns; (b) low-, and (c) high-magnification TEM images; (d) HRTEM image of the selected area marked with a yellow rectangle in (c); (e and f) the corresponding elemental mapping of In and S in the same area; (g) EDX spectrum.

3.2 Effects of precursor ratio on the morphology of In_2S_3 nanocrystals

In order to investigate the influence of molar ratio of reactants on the morphology of In_2S_3 nanocrystals, the morphologic variety at different molar ratios of indium nitrate to thioacetamide was examined by SEM (Figure 3). When molar ratio of indium nitrate to thioacetamide is 1:1.5, the product is composed of the smallest flower-like nanostructures illustrated in Figure 3a, with a diameter of about 400-650 nm. When the molar ratio is further decreased to 1:3.5, the diameters are 550-650 nm (Figure 3b). When the molar ratio is 1:4.5, the diameters are 400-450 nm (Figure 3c). When the molar ratio is 1:6, the diameters are 300-350 nm (Figure 3d). These SEM results indicate that the general flower-like morphology of these In_2S_3 nanostructures is almost the same. However, it is apparent that

the diameter of the individual flowers can be controlled by changing the concentration of thioacetamide. All the above samples of In_2S_3 have the same crystal structure, as confirmed by XRD (Figure 4).

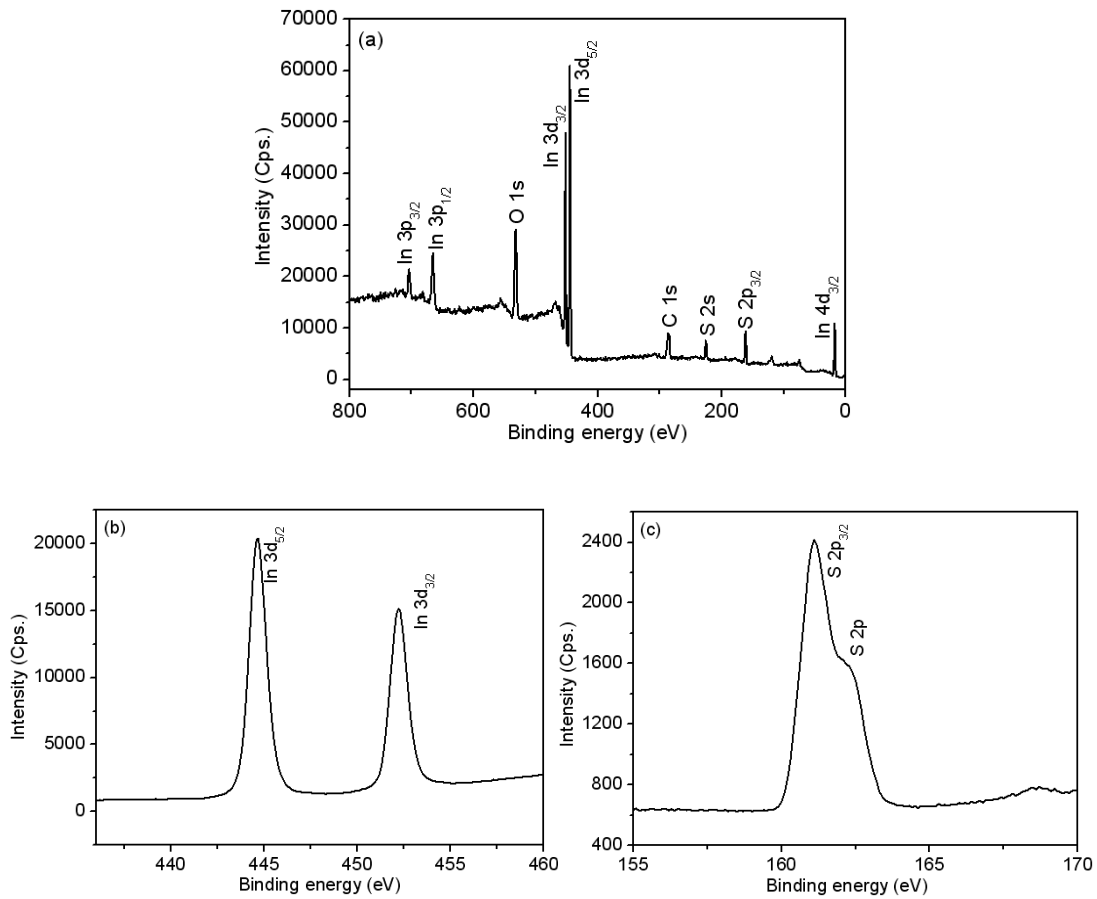


Figure 2. XPS analysis of the sample In_2S_3 -1:6: (a) survey spectrum, (b) In 3d and (c) S 2p bonding-energy spectrum.

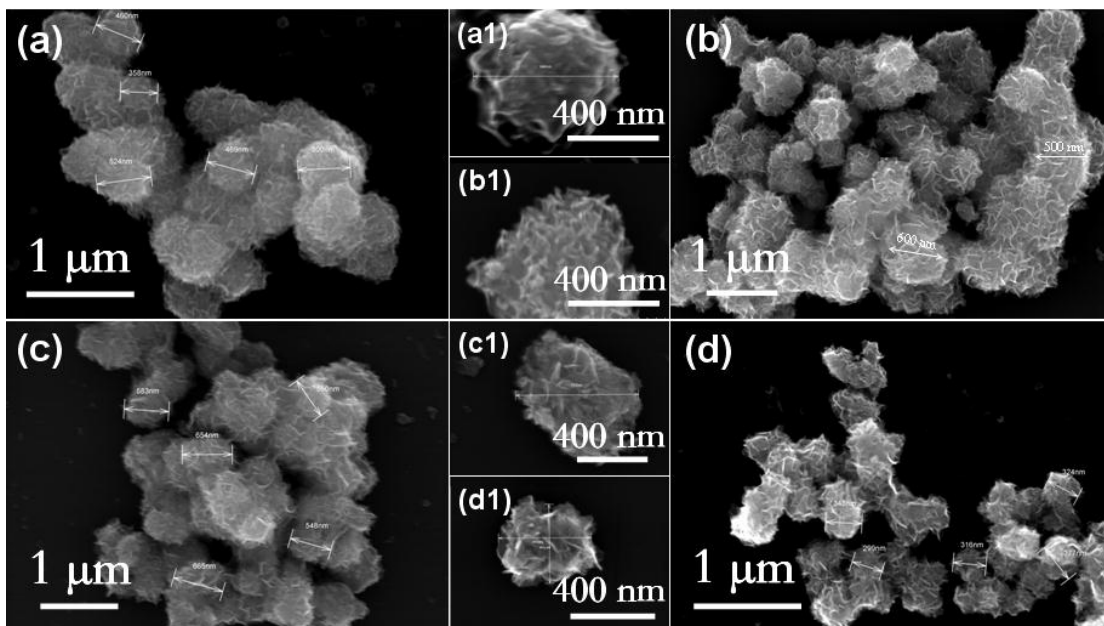


Figure 3. SEM images of the prepared products under different $\text{In}(\text{NO}_3)_3/\text{C}_2\text{H}_5\text{NS}$ molar ratios: (a, a₁) 1:1.5, (b, b₁) 1:3.5, (c, c₁) 1:4.5, (d, d₁) 1:6.

3.3 Growth mechanism of In_2S_3 nanoflowers

As is well known, the morphology of nanocrystals can be determined by their intrinsic crystal structures [26]. Figures 1a and 1d demonstrate that the crystal structure of the prepared In_2S_3 is cubic close packing. Thus, In_2S_3 crystals usually present a morphology of 2D nanoplates. High concentration of In^{3+} and S^{2-} could lead to fast nucleation and congregation of In_2S_3 in the early stages, resulting in sphere-like cores, which could then serve as heterogeneous nucleation sites, providing high-energy sites for crystalline growth. Then a secondary nucleation would be favored, and cubic angular protuberances would grow into nanopetals combining with the remaining primary particles, finally forming the 3D flower-like hierarchitectures, a process which is similar to that described as “the terrace-step-kink model” [27]. This is similar to the formation process of those flower-like nanocrystals reported previously, such as CoS [28], CuO [29], TiS_2 [30], In_2O_3 [31], $\text{AlO}(\text{OH})$ [32], ZnO [33], Bi_2MoO_6 [34], $\text{Ni}(\text{OH})_2$ [35] and so on.

We observed that the sizes of In_2S_3 nanoflowers decreased with increasing the concentration of $\text{C}_2\text{H}_5\text{NS}$ (Figure 4). This can be explained as follows. The thioacetamide ions can be easily absorbed on the In_2S_3 surface, which slows down the rate of growth units moving to the growing crystal surface. This contributes to the growth units having enough time to move towards the lowest or favorite energy position. Thermodynamics plays a dominant role in this process. The adsorbed thioacetamide ions can stabilize and protect the In_2S_3 exposed facet; this will be helpful to form a bigger nanoplate (Figure 4a). However, as the concentration of thioacetamide increases, the higher concentration of S^{2-} leads to easier nucleation and a faster reaction rate, resulting in a lack of time to age and thus producing small sized nanoflowers (Figure 4d). In this process kinetic growth dominates the strongest effect. This indicates that there is a synergistic effect between thioacetamide ions protecting the crystal facets and the nucleation rate, causing thioacetamide to tune the growth of In_2S_3 nanoplates. Therefore, the growth rate and morphology of flower-like In_2S_3 crystals can be controlled by adjusting the thioacetamide concentration in the mixed solvent.

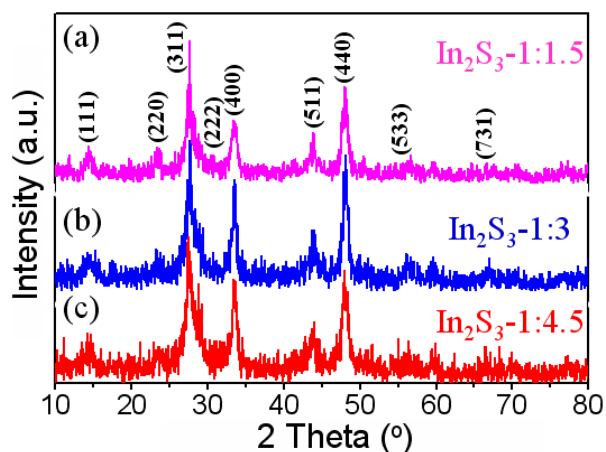


Figure 4. XRD of the prepared final In_2S_3 products under different $\text{In}(\text{NO}_3)_3/\text{C}_2\text{H}_5\text{NS}$ molar ratios: (a) 1:1.5, (b) 1:3.5, (c) 1:4.5.

3.4 Optical properties

The optical property of the obtained In_2S_3 nanoflowers was investigated by an UV-vis absorption spectrophotometer. As shown in Figure 5, the absorption edges of the In_2S_3 nanoflowers were found between 652 and 630 nm, corresponding to the absorption edge of a semiconductor material. It is interesting that the absorption edges for all samples were very close to each other. However, the absorption edge for the samples from In_2S_3 -1:1.5 to In_2S_3 -1:6 showed a small blue shift, which can be attributed to the quantization size effect of the In_2S_3 nanoflowers [36]. For a crystalline semiconductor, the optical absorption near the band edge follows the equation $\alpha h\nu = A(h\nu - E_g)^{n/2}$, where α , ν , E_g and A are the absorption coefficient, the light frequency, the band gap and a constant, respectively. Among them, n decides the characteristics of the transition in a semiconductor [37]. The band gaps are calculated to be about 1.90, 1.92, 1.97, and 1.95 eV for In_2S_3 -1:1.5, In_2S_3 -1:3, In_2S_3 -1:4.5 and In_2S_3 -1:6, respectively, from the onset of the absorption edge (inset of Figure 5). It should be noted that those values are smaller than the one reported in our previous studies (2.00 eV) [15]. The main reason may attribute to the large size of In_2S_3 nanoflowers. This indicates that the In_2S_3 nanoflowers have a suitable band gap for photocatalytic decomposition of organic contaminants under visible light irradiation.

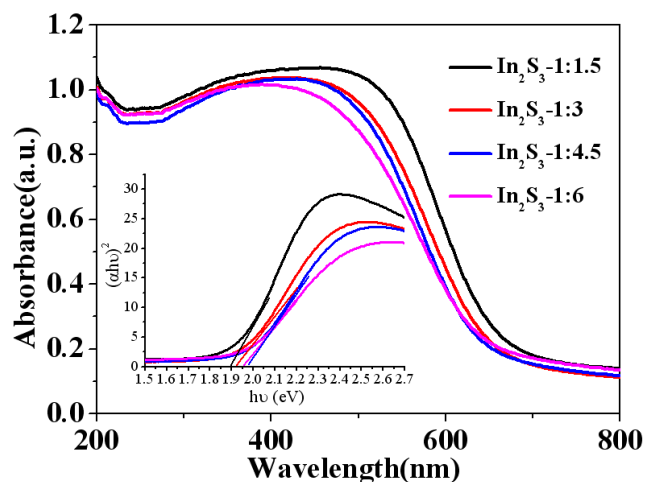


Figure 5. UV-vis diffuse reflectance spectra of In_2S_3 nanoflowers.

3.5 Photocatalytic performance of In_2S_3 nanoflowers

In order to study the photocatalytic degradation properties of the prepared In_2S_3 samples, methylene blue was used as a probe pollutant to investigate the photocatalytic performance of In_2S_3 nanoflowers (In_2S_3 -1:6 sample, for example). The maximum absorptive energy of methylene blue was at 664 nm. Figure 6 shows that the absorptive intensity of methylene blue at 664 nm gradually decreased with prolonging the irradiation time, when the mixed solution of methylene blue and In_2S_3 nanoflowers was exposed to visible light irradiation by a sodium vapor lamp at room temperature. This result indicates that methylene blue underwent degradation behavior under the catalysis of In_2S_3 nanoflowers. If the degradation ratio is defined as the ratio between the decreased absorptive intensity and that of the initial methylene blue solution, the degradation ratio was about 85% when the mixed solution was irradiated for 3 h. This implies that the prepared In_2S_3 nanoflowers have good photocatalytic activity for methylene blue and are likely to be an efficient photocatalyst. As to the photocatalytic mechanism of In_2S_3 nanoflowers on methylene blue, we assume that the electron injection from photoexcited methylene blue molecules to In_2S_3 nanoflowers leads to oxidative decomposition of the consequently electron-deficient methylene blue. To the best of our knowledge, the photocatalytic performance of β - In_2S_3 nanoflowers has not been reported and the catalytic mechanism of β - In_2S_3 has not been well understood until now.

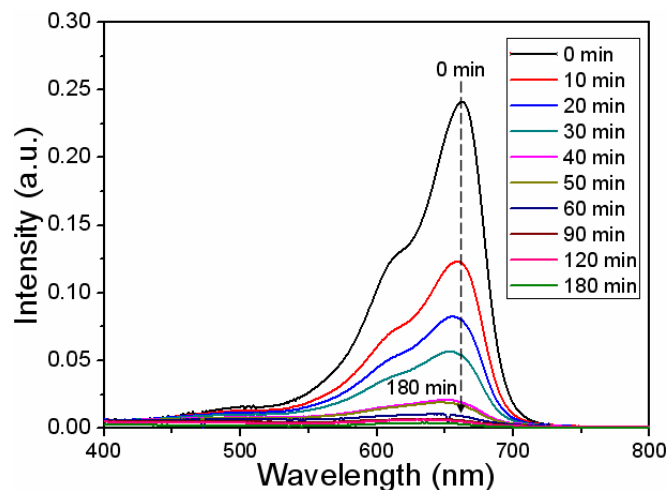


Figure 6. Time-dependent UV-vis absorption spectra of methylene blue (5mg/L) degradation in In_2S_3 nanoflowers under visible light irradiation. [Conditions: MB concentration – 5mg/L; amount of catalyst – 400 mg/L].

4. Conclusion

In summary, we have reported a simple method to prepare flower-like β - In_2S_3 hierarchitectures by a solution-phase process, using $(\text{In}(\text{NO}_3)_3)_2$ and thioacetamide as the precursors. The XRD analysis confirmed that the In_2S_3 nanoflowers are in cubic phase. The SEM and TEM analysis revealed that the products are flower-like in shape, with a diameter from 300 nm to 650 nm. On the basis of the structural and morphological studies, a possible growth mechanism has been proposed to explain the formation of the In_2S_3 nanoflowers. The compositional analysis made by EDX and XPS measurements confirmed that the stoichiometric In/S ratio is approximately 2:3, which indicates high-purity In_2S_3 . The UV-vis DRS measurements demonstrated that the samples have the band gap from 1.90 to 1.97 eV

and slightly change with varying crystal sizes. Thus, the narrow band gap of our samples combined with the pronounced catalytic activity for methylene blue degradation suggests that it is a highly efficient photocatalyst.

5. Acknowledgment

One of the authors (R.S.) thanks Sultan Qaboos University for financial support for this work under a SQU Internal Research Grant (IG/SCI/CHEM/14/02).

References

- Li, J. and Wang, L.W., Shape effects on electronic states of nanocrystals. *Nano Lett.*, 2003, **3**, 1357-1363.
- Qi, K.Z., Yang, J.Q., Fu, J.Q., Wang, G.H., Zhu, L.J. and Zheng, W.J., Morphology-controllable ZnO rings: ionic liquid-assisted hydrothermal synthesis, growth mechanism and photoluminescence properties. *Cryst. Eng. Comm.*, 2013, **15**, 6729-6735.
- Ferancova, A., Rengaraj, S., Kim, Y., Vijayalakshmi, S., Labuda, J., Bobacka, J. and Sillanpää, M. Electrochemical study of novel nanostructured In₂S₃ and its effect on oxidative damage to DNA purine bases. *Electrochim. Acta.*, 2013, **92**, 124-131.
- Xiao, Y.M., Wu, J., Lin, J.Y., Tai, S.Y. and Yue, G.T. Pulse electrodeposition of CoS on MWCNT/Ti as a high performance counter electrode for a Pt-free dye-sensitized solar cell. *J. Mater. Chem. A.*, 2013, **1**, 1289-1295.
- Wang, H., Liang, Q.Q., Wang, W.J., An, Y.R., Li, J.H. and Guo, L. Preparation of flower-like SnO₂ nanostructures and their applications in gas-sensing and lithium storage. *Cryst. Growth Des.*, 2011, **11**, 2942-2947.
- Wang, Q.H., Jiao, L.F., Du, H.M., Yang, J.Q., Huan, Q.N., Peng, W.X., Si, Y.H., Wang, Y.J. and Yuan, H.T. Facile synthesis and superior supercapacitor performances of three-dimensional cobalt sulfide hierarchitectures. *Cryst. Eng. Comm.*, 2011, **13**, 6960-6963.
- Helmut, C. and Markus, A. Mesocrystals: Inorganic superstructures made by highly parallel crystallization and controlled alignment. *Angew. Chem. Int. Ed.*, 2005, **44**, 5576-5591.
- Yang, J., Lin, C.K., Wang, Z.L. and Lin, J. In(OH)₃ and In₂O₃ nanorod bundles and spheres: microemulsion-mediated hydrothermal synthesis and luminescence properties. *Inorg. Chem.*, 2006, **45**, 8973-8979.
- Kim, W.-T. and Kim, C.-D. Optical energy gaps of In₂S₃ thin films grown by spray pyrolysis. *J. Appl. Phys.*, 1986, **60**, 2631-2633.
- Jayakrishnan, R., Sebastian, T., John, T.T., Kartha, C.S. and Vijayakumar, K.P. Photoconductivity in sprayed β-In₂S₃ thin films under sub-band-gap excitation of 1.96 eV. *J. Appl. Phys.*, 2007, **102**, 043109.
- Calixto-Rodriguez, M., Tiburcio-Silver, A., Ortiz, A. and Sanchez-Juarez, A. Optoelectronic properties of indium sulfide thin films prepared by spray pyrolysis for photovoltaic applications. *Thin Solid Films.*, 2005, **480-481**, 133-137.
- Yang, M.Q., Weng, B. and Xu, Y.J. Synthesis of In₂S₃-CNT nanocomposites for selective reduction under visible light. *J. Mater. Chem. A.*, 2014, **2**, 1710-1720.
- Liu, G.D., Jiao, X. L., Qin, Z.H. and Chen, D.R. Solvothermal preparation and visible photocatalytic activity of polycrystalline β-In₂S₃ nanotubes. *Cryst. Eng. Comm.*, 2011, **13**, 182-187.
- Du, W.M., Zhu, J., Li, S. X. and Qian, X.F. Ultrathin β-In₂S₃ nanobelts: shape-controlled synthesis and optical and photocatalytic properties. *Cryst. Growth Des.*, 2008, **8**, 2130-2136.
- Rengaraj, S., Venkataraj, S., Tai, C.W., Kim, Y., Repo, E. and Sillanpää, M. Self-assembled mesoporous hierarchical-like In₂S₃ hollow microspheres composed of nanofibers and nanosheets and their photocatalytic activity. *Langmuir*, 2011, **27**, 5534-5541.
- He, Y., Li, D., Xiao, G., Chen, W., Chen, Y., Sun, M., Huang, H. and Fu, X. A New application of nanocrystal In₂S₃ in efficient degradation of organic pollutants under visible light irradiation. *J. Phys. Chem. C*, 2009, **113**, 5254-5262.
- Liu, Y., Xu, H.Y. and Qian, Y. Double-source approach to In₂S₃ single crystallites and their electrochemical properties. *Cryst. Growth Des.*, 2006, **6**, 1304-1307.
- Datta, A., Sinha, G., Panda, S.K. and Patra, A. Growth, optical, and electrical properties of In₂S₃ zigzag nanowires. *Cryst. Growth Des.*, 2009, **1**, 427-431.
- Kim, Y.H., Lee, J.H., Shin, D.W., Park, S. M., Moon, J.S., Nam, J.G. and Yoo, J.B. Synthesis of shape-controlled β-In₂S₃ nanotubes through oriented attachment of nanoparticles. *Chem. Commun.*, 2010, **46**, 2292-2294.
- Du, W.M., Zhu, J., Li, S.X. and Qian, X.F. Ultrathin β-In₂S₃ nanobelts: shape-controlled synthesis and optical and photocatalytic properties. *Cryst. Growth Des.*, 2008, **7**, 2130-2136.
- Liu, Y., Zhang, M., Gao, Y.Q., Zhang, R. and Qian, Y.T. Effect of a phase-transfer catalyst on the chemical modification of poly(vinyl chloride) by substitution with thiocyanate as a nucleophile. *Mater. Chem. Phys.*, 2007, **101**, 362-366.
- Chai, B., Zeng, P., Zhang, X.H., Mao, J., Zan, L. and Peng, T.Y. Walnut-like In₂S₃ microspheres: ionic liquid-assisted solvothermal synthesis, characterization and formation mechanism. *Nanoscale.*, 2012, **4**, 2372-2377.
- Datta, A., Gorai, S., Ganguli, D. and Chaudhuri, S. Surfactant-assisted synthesis of In₂S₃ dendrites and their characterization. *Mater. Chem. Phys.*, 2007, **102**, 195-200.

24. Revathi, N., Prathap, P., Subbaiah, Y. P.V. and Ramakrishna Reddy, K.T. Substrate temperature dependent physical properties of In_2S_3 films. *J. Phys. D: Appl. Phys.*, 2008, **41**, 155404.
 25. Wei, C.Y., Guo, W., Yang, J.Q., Fan, H.M., Zhang, J. and Zheng, W.J. Facile solvothermal synthesis of 3D flowerlike $\beta\text{-In}_2\text{S}_3$ microspheres and their photocatalytic activity performance. *RSC Adv.*, 2014, **4**, 50456-50463.
 26. Du, W.M., Qian, X. F., Niu, X.S. and Gong, Q. Symmetrical six-horn nickel diselenide nanostars growth from oriented attachment mechanism. *Cryst. Growth Des.*, 2007, **7**, 2733-2737.
 27. Burton, W.K., Cabrera, N. and Frack, F.C. The growth of crystals and the equilibrium structure of their surfaces. *Philos. Trans. R. Soc. A.*, 1951, **243**, 299-358.
 28. Qi, K.Z., Yu, J. and Chen, K. A simple surfactant-free route for preparation of flower-like crystals of CoS with hierarchitectures. *Cryst. Res. Technol.*, 2013, **48**, 1083-1086.
 29. Cheng, Z.P., Xu, J.M., Zhong, H., Chu, X.Z. and Song, J. Hydrogen peroxide-assisted hydrothermal synthesis of hierarchical CuO flower-like nanostructures. *Mater. Lett.*, 2011, **65**, 2047-2050.
 30. Prabakar, S., Bumby, C.W. and Tilley, R.D. Liquid-phase synthesis of flower-like and flake-like titanium disulfide nanostructures. *Chem. Mater.*, 2009, **21**, 1725-1730.
 31. Wang, C.Q., Chen, D.R. and Jiao, X.L. Flower-like In_2O_3 nanostructures derived from novel precursor: synthesis, characterization, and formation mechanism. *J. Phys. Chem. C.*, 2009, **113**, 7714-7718.
 32. Yu, X.X., Yu, J.G., Cheng, B. and Jaroniec, M. Synthesis of hierarchical flower-like AlOOH and $\text{TiO}_2/\text{AlOOH}$ superstructures and their enhanced photocatalytic properties. *J. Phys. Chem. C.*, 2009, **113**, 17527-17535.
 33. Li, B.X. and Wang, Y.F. Facile synthesis and enhanced photocatalytic performance of flower-like ZnO hierarchical microstructures. *J. Phys. Chem. C.*, 2010, **114**, 890-896.
 34. Tian, G.H., Chen, Y.J., Zhou, W., Pan, K., Dong, Y.Z., Tian, C.G. and Fu, H.G. Facile solvothermal synthesis of hierarchical flower-like Bi_2MoO_6 hollow spheres as high performance visible-light driven photocatalysts. *J. Mater. Chem.*, 2011, **21**, 887-892.
 35. Zhu, L.P., Liao, G.H., Yang, Y., Xiao, H.M., Wang, J.F. and Fu, S.Y. Self-assembled 3D flower-like hierarchical b-Ni(OH)₂ hollow architectures and their in situ thermal conversion to NiO. *Nanoscale Res Lett.*, 2009, **4**, 550-557.
 36. Tawkaew, S., Fujishiro, Y., Yin, S. and Sato, T. Synthesis of cadmium sulfide pillared layered compounds and photocatalytic reduction of nitrate under visible light irradiation. *Colloids Surf. A.*, 2001, **179**, 139-144.
 37. Zhang, J., Shi, F.J., Chen, D.F., Gao, J.M., Huang, Z.X., Ding, X.X. and Tang, C.C. Self-assembled 3-D architectures of BiOBr as a visible light-driven photocatalyst. *Chem. Mater.*, 2008, **20**, 2937-2941.
-

Received 8 September 2014

Accepted 25 September 2014